PHOTONICS Research

# Efficient intensity noise suppression for all-solid-state CW lasers

Jiliang Qin,[1,2,†] Weina Peng,[1,†] Jing Su,[1,2] Xiaojun Jia,[1,2,3] Huadong Lu,[1,2,*] and Kunchi Peng[1,2]

[1]State Key Laboratory of Quantum Optics Technologies and Devices, Institute of Opto-Electronics, Shanxi University, Taiyuan 030006, China
[2]Collaborative Innovation Center of Extreme Optics, Shanxi University, Taiyuan 030006, China
[3]e-mail: jiaxj@sxu.edu.cn
[†]These authors contributed equally to this work.
*Corresponding author: luhuadong@sxu.edu.cn

Received 18 August 2026; revised 3 October 2026; accepted 3 October 2026; posted 5 October 2026 (Doc. ID 614626); published 19 November 2026

**The excessive intensity noise of laser source is a stubborn impediment to precision measurement. Despite decades of efforts to develop numerous approaches to reduce laser noise, the problem of high noise levels in the low-frequency band of all-solid-state lasers has remained unsolved. To address this challenge, we establish a transfer function model for all-solid-state lasers with pump-current optoelectronic feedback and reveal the intrinsic relationship between the key parameters of laser dynamics and feedback control. Based on this model, we find that synergistically increasing nonlinear loss and loop bandwidth effectively enhances the maximum allowable open-loop gain and then improves the noise suppression capability. On this basis, we propose a noise suppression method integrating nonlinear loss with a high-bandwidth GaN-based feedback circuit. Then, the presented model and method are validated in an all-solid-state single-frequency CW 1064 nm laser with an output power of 30 W. When the bandwidth of the GaN-based feedback circuit and the nonlinear loss rate are 30 MHz and $5.6 \times 10^6$/s, respectively, more than 16 dB of low-frequency noise suppression is successfully achieved. The experimental results are in good agreement with the theoretical prediction. This work provides a theoretical framework for understanding and overcoming the gain-phase trade-off in optoelectronic feedback systems. Beyond all-solid-state lasers, the model offers a general design guideline for low-noise, high-power coherent sources, with direct implications for quantum optics, precision metrology, and gravitational wave detection.** © 2026 Chinese Laser Press

https://doi.org/10.1364/PRJ.614626

## 1. INTRODUCTION

Low-noise all-solid-state single-frequency continuous-wave (CW) lasers have become a central requirement in the cutting-edge fields, including gravitational wave detection [1–4], quantum optics [5–9], and cold atom physics [10,11]. Especially, in precise measurement systems, the ultimate precision limit is directly determined by the intensity noise and output power of the laser. However, for a free-running all-solid-state single-frequency laser, the noise characteristics exhibit a distinct frequency dependence. In the mid-to-high frequency range, the intensity noise can approach the shot-noise-limit (SNL), owing to the dominance of stimulated emission quantum fluctuations and the cavity filtering effect. In contrast, during the process of achieving laser generation through particle number inversion, the strong nonlinear coupling between the population inversion and the intracavity photons can form a resonant relaxation oscillation (RRO), which makes the intensity noise higher than the SNL. At the same time, the generated laser can directly inherit the intensity noise from the pump source below the frequency of RRO [12–15]. Such low-frequency noise severely limits the signal-to-noise ratio and resolution of the optical precision measurements [16].

To address this challenge, some feedback loops based on acousto-optic or electro-optic modulators were employed to stabilize the amplitude of the output laser beam for suppressing the intensity noise [17,18]. However, it is difficult to implement at high power levels for the modulators due to limited power handling capacity. The mode cleaner can also be used to filter out the intensity noise of the laser [19]. However, it offers little suppression in the low-frequency range and introduces significant insertion loss. In addition, these techniques do not alter the intrinsic noise characteristics of the laser itself. To genuinely reduce the intensity noise of the laser itself, some new technologies, including introducing the nonlinear losses into the laser resonator to increase damping and suppress the RRO [20] and manipulating the stimulated emission rate to reduce the intensity noise [21], were developed. However, these technologies have almost no effect at low frequencies, and their

capacity for noise suppression is severely limited. Therefore, a technique that can directly target the source of low-frequency noise without sacrificing output power is highly desirable [22]. To address this demand, pump-current optoelectronic feedback (hereafter referred to as optoelectronic feedback) of the laser, which modulates the pump current, offers a promising approach to directly suppress low-frequency noise at its source. This method was first adopted in 1990 to suppress the RRO [13]. Since the laser's noise transfer function exhibits a phase shift of approximately 180° at the RRO frequency [23,24], in 2001, our group introduced a phase-advance compensation to pump-current optoelectronic feedback. This reduced RRO peak noise by 25 dB, but low-frequency noise was reduced by only about 4 dB [24]. In the same year, we analyzed for the first time the intensity noise and pump-transfer characteristics of an all-solid-state single-frequency laser and its intracavity frequency-doubled counterpart. Even under the overdamped condition, optoelectronic feedback reduced the noise of the frequency-doubled laser by only about 7 dB [25]. Since then, the phase margin limitation imposed by the laser's RRO has remained unresolved, and it becomes progressively more severe at higher output powers. Previous approaches relied on empirical phase-advance filtering [24,25], which is effective only over a narrow band and cannot fundamentally relax the gain-phase trade-off. As a result, progress in applying optoelectronic feedback to all-solid-state lasers has been slow, and to our knowledge it has not been widely adopted in commercial high-power single-frequency lasers.

To overcome this limitation, a unified transfer function model that incorporates the feedback circuit response with the laser dynamics of the all-solid-state laser is established in this paper. This model reveals that the failure of conventional feedback stems from the phase margin erosion by the fatal interaction between the laser's RRO and the feedback circuit's limited bandwidth. This severe phase margin erosion forces the loop gain impractically low and fundamentally limits noise suppression. Guided by this insight, by analyzing the relationship between the nonlinear loss rate and phase margin, we propose, for the first time to our knowledge, a method that synergistically integrates nonlinear loss with optoelectronic feedback, where the nonlinear loss is used to expand the phase margin and enable high-gain feedback in the underdamped regime of a high-power laser. And a validation experiment for the model and method is conducted on an all-solid-state single-frequency CW 1064 nm laser with an output power of 30 W. The low-frequency noise is suppressed an order of magnitude better than the conventional methods. The experimental results are in good agreement with the theoretical predictions. Beyond this specific demonstration, this work provides a general design principle for integrated laser-and-feedback systems: engineering the damping of the laser can relax the gain-phase trade-off and enable a higher feedback gain.

## 2. THEORY OF OPTOELECTRONIC FEEDBACK AND NOISE SUPPRESSION MECHANISMS

### A. Principle of Optoelectronic Feedback Control

The optoelectronic feedback system of an all-solid-state laser actively suppresses intensity noise by forming a negative feedback control loop that monitors real-time fluctuations in the output power and modulates the pump current accordingly. The feedback-loop system primarily consists of the laser, a photodetector (PD), and the current driver. The open-loop transfer function determines both the stability and the noise suppression performance of the system. In the following, the transfer functions of the key components are derived.

The low-frequency intensity noise of all-solid-state lasers predominantly originates from the pump source; therefore, we focus on the transfer function of the pump noise. For a four-level CW laser system, the dynamics of the population inversion density $N(t)$ and the intracavity fundamental photon density $S(t)$ are governed by the rate equations:

$$\frac{\mathrm{d}N(t)}{\mathrm{d}t} = R_p(t) - \gamma_N N(t) - GN(t)S(t), \tag{1}$$

$$\frac{\mathrm{d}S(t)}{\mathrm{d}t} = GN(t)S(t) - 2\kappa S(t), \tag{2}$$

where $R_p(t)$ is the pumping rate (proportional to the pump intensity), $\gamma_N$ is the spontaneous emission rate of the upper laser level, $G$ is the stimulated emission coefficient, and $2\kappa = 2\kappa_m + 2\kappa_l$ is the total cavity decay rate, with $2\kappa_m$ and $2\kappa_l$ denoting the output coupling rate and the intracavity loss rate, respectively.

Under steady-state operation, setting $\frac{\mathrm{d}N(t)}{\mathrm{d}t} = 0$, $\frac{\mathrm{d}S(t)}{\mathrm{d}t} = 0$ yields the equilibrium conditions:

$$GN_0 = 2\kappa, \tag{3}$$

$$R_{p0} = \gamma_N N_0 + 2\kappa S_0. \tag{4}$$

We apply small-signal linearization processing around the operating point $(N_0, S_0)$, that is, $N(t) = N_0 + \delta N(t)$, $S(t) = S_0 + \delta S(t)$, $R_p(t) = R_{p0} + \delta R_p(t)$. It is worth noting that pump depletion and gain saturation effects are implicitly included in the steady-state operating point $(N_0, S_0)$ determined by Eq. (4). The small-signal analysis focuses on the linearized response of fluctuations around this equilibrium, which is a standard and valid approach for analyzing the frequency response of laser oscillators under weak modulation. Then, we substitute Eqs. (1) and (2) in combination with the steady-state conditions:

$$\frac{\mathrm{d}\delta N}{\mathrm{d}t} = \delta R_p - (\gamma_N + GS_0)\delta N - 2\kappa\delta S, \tag{5}$$

$$\frac{\mathrm{d}\delta S}{\mathrm{d}t} = GS_0\delta N. \tag{6}$$

Transforming into the frequency domain via Laplace transform yields

$$[s^2 + (\gamma_N + GS_0)s + 2\kappa GS_0]\delta S(s) = GS_0\delta R_p(s), \tag{7}$$

where $s = j\omega$ is the complex frequency and $\omega$ is the angular frequency. The dynamic transfer function from pump disturbance to fundamental output is then

$$H_L(s) = \frac{2\eta_a\kappa_m\lambda_p\delta S(s)}{\lambda_0\delta R_p(s)} = \frac{2\eta_a\kappa_m GS_0\frac{\lambda_p}{\lambda_0}}{s^2 + (\gamma_N + GS_0)s + 2\kappa GS_0}. \tag{8}$$

Here, $\eta_a$ is the absorption efficiency of the pump laser, and $\lambda_p$ and $\lambda_0$ are the wavelengths of the pump and fundamental laser, respectively. From the standard second-order transfer

function, the RRO angular frequency and the damping rate are obtained as

$$\omega_r = \sqrt{2\kappa G S_0}, \tag{9}$$

$$\gamma = G S_0 + \gamma_N. \tag{10}$$

With the laser transfer function established, we now turn to the other components in the feedback loop. To avoid introducing additional phase shifts, a high-bandwidth, low-noise photodetector (>100 MHz) is employed. Within the target frequency band, its delay is negligible, and its transfer function can be approximated as a proportional gain:

$$H_{\mathrm{PD}}(j\omega) = -\eta_{\mathrm{PD}} \cdot R, \tag{11}$$

where $R$ is the responsivity of the high-bandwidth photodetector (V/W) and $\eta_{\mathrm{PD}}$ is the ratio of the power incident on the photodetector to the total fundamental output power.

For the current feedback driver, conventional silicon-based MOSFETs suffer from parasitic capacitance and limited carrier mobility, causing a sharp roll-off in transconductance gain $g_m$ at high frequencies. Their response behaves as a low-pass filter with a −3 dB bandwidth $f_d$ typically within 1 MHz, and the transfer function is given by

$$H_c(j\omega) = \frac{\eta_L g_m}{1 + \frac{j\omega}{2\pi f_d}}, \tag{12}$$

where $\eta_L$ is the slope efficiency of the laser diode (LD). The total open-loop transfer function of the optoelectronic feedback system is

$$H_o(j\omega) = \frac{-2\kappa_m G S_0 \eta_L \eta_a \eta_{\mathrm{PD}} R g_m \frac{\lambda_p}{\lambda_0}}{(\omega_r^2 + j\omega\gamma - \omega^2)\left(1 + \frac{j\omega}{2\pi f_d}\right)}, \tag{13}$$

with $A = 2\kappa_m G S_0 \eta_L \eta_a \eta_{\mathrm{PD}} R g_m \frac{\lambda_p}{\lambda_0}$. The corresponding open-loop amplitude and phase responses are given as follows:

$$|H_o(j\omega)| = \frac{A}{\sqrt{(\omega_r^2 - \omega^2)^2 + (\omega\gamma)^2}\sqrt{1 + \left(\frac{\omega}{2\pi f_d}\right)^2}}, \tag{14}$$

$$\angle H_o(j\omega) = -\arctan\left(\frac{\omega}{2\pi f_d}\right) - \arctan\left(\frac{\omega\gamma}{\omega_r^2 - \omega^2}\right). \tag{15}$$

According to Eqs. (14) and (15), for a single-frequency laser in steady state, using the parameters in Table 1, the calculated normalized gain and phase response are shown in Fig. 1. The curves (i) and (iv) in Fig. 1 are the results of using silicon-based MOSFETs, which reveal that the silicon driver introduces a significant phase lag at frequencies above 500 kHz. As a result, the phase margin of the feedback loop is severely reduced. To ensure stable operation, a phase margin of at least 30° is typically required; satisfying this condition forces the loop gain to be kept at a very low level. Consequently, the noise suppression capability is severely limited. This gain-phase trade-off is the fundamental reason why conventional optoelectronic feedback performs poorly in all-solid-state lasers.

To overcome this limitation, first, we replace the silicon driver with a high-bandwidth GaN FET. GaN devices feature

**Table 1. Key System Parameters for the Calculations Presented in Fig. 1**

| Parameter | Value |
|---|---|
| Stimulated emission rate ($GS_0$) | $2 \times 10^5$/s |
| Spontaneous emission rate ($\gamma_N$) | $10^4$/s |
| Nonlinear loss rate ($2\kappa_n$) | $6 \times 10^6$/s |
| Output coupling rate ($2\kappa_m$) | $10^8$/s |
| Intracavity loss rate ($2\kappa_l$) | $10^7$/s |
| Si-based driver bandwidth ($f_d$) | 800 kHz |
| GaN driver bandwidth ($f_{\mathrm{GaN}}$) | 30 MHz |

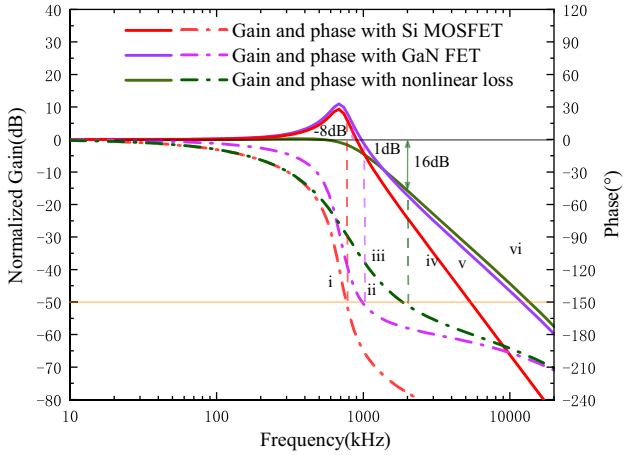



**Fig. 1.** Open-loop gain-frequency and phase-frequency responses. (i) Phase response with Si-based driver; (ii) phase response with GaN driver; (iii) phase response with GaN driver and nonlinear loss; (iv) normalized noise power gain without feedback; (v) normalized noise power gain with GaN driver; (vi) normalized noise power gain with GaN driver and nonlinear loss.

extremely low parasitic capacitance and gate charge, offering a small-signal −3 dB bandwidth $f_{\mathrm{GaN}}$ exceeding 30 MHz. Within our target band (<5 MHz), the GaN high-bandwidth circuit introduces negligible phase shift and can be approximated as an ideal proportional element:

$$H_c(j\omega) = \frac{\eta_L g_m}{1 + \frac{j\omega}{2\pi f_{\mathrm{GaN}}}} \approx \eta_L g_m. \tag{16}$$

Therefore, the open-loop amplitude frequency function of the laser is approximately

$$|H_o'(j\omega)| \approx \frac{A}{\sqrt{(\omega_r^2 - \omega^2)^2 + (\omega\gamma)^2}}. \tag{17}$$

The phase frequency function is approximated as

$$\angle H_o'(j\omega) \approx -\arctan\left(\frac{\omega\gamma}{\omega_r^2 - \omega^2}\right) - \pi. \tag{18}$$

The phase and normalized gain curves are shown as curves (ii) and (v) in Fig. 1. According to this Bode plot, although the gain margin is improved compared to silicon-based MOSFETs, the corresponding open-loop gain is only about 1 dB when the phase is −150°. This would excite large

oscillation noise even with a small feedback gain, so it still cannot effectively suppress noise. To overcome this limitation, we observed that the nonlinear loss introduced by an intracavity frequency-doubling crystal can dramatically enhance the gain margin.

### B. Nonlinear Loss and Gain Margin Enhancement

When a nonlinear crystal for second-harmonic generation (SHG) is inserted into the cavity, the fundamental wave generates a second-harmonic field through a parametric conversion process. This frequency-doubling process depletes the fundamental photons at a rate quadratic to the fundamental intensity, which not only steepens the energy gradient in the fundamental frequency laser mode competition but also enhances the single-frequency stability of the laser. More importantly, this nonlinear consumption mechanism manifests as a nonlinear loss term in the photon rate equation. The instantaneous loss rate is proportional to the number of photons inside the cavity: $2\kappa_n = \mu S(t)$, where $\mu$ is the nonlinear loss coefficient. Consequently, the photon rate equation is modified as

$$\frac{\mathrm{d}S(t)}{\mathrm{d}t} = GN(t)S(t) - 2\kappa S(t) - \mu S(t)^2. \tag{19}$$

The steady-state condition becomes $GN_0 = 2\kappa + \mu S_0$. After the same small signal linearization and Laplace transform as described above,

$$[s^2 + (\gamma_N + GS_0 + \mu S_0)s + 2\kappa GS_0 + \mu S_0(\gamma_N + 2GS_0)]\delta S(s) = GS_0\delta R_p(s). \tag{20}$$

Therefore, the dynamic transfer function of the pump laser disturbance caused by the output fundamental frequency laser is corrected to

$$H_L'(s) = \frac{2\eta_a\kappa_m GS_0\frac{\lambda_p}{\lambda_0}}{s^2 + (\gamma_N + GS_0 + \mu S_0)s + 2\kappa GS_0 + \mu S_0(\gamma_N + 2GS_0)}. \tag{21}$$

The RRO angular frequency of fundamental frequency laser is

$$\omega_r' = \sqrt{2\kappa GS_0 + 2\kappa_n(2GS_0 + \gamma_N)}. \tag{22}$$

The damping rate is

$$\gamma' = 2\kappa_n + GS_0 + \gamma_N. \tag{23}$$

The nonlinear loss directly and substantially increases the system damping rate, rapidly quenching energy oscillations between the population inversion and the fundamental-frequency optical field, thereby suppressing the RRO peak. In contrast, linear loss can only slightly change damping by affecting $S_0$. Thus, the introduction of a small amount of SHG nonlinear loss ensures sufficient fundamental output power, suppresses mode competition, and more importantly, significantly enhances damping.

The open-loop transfer function of the feedback system is updated to

$$H_o''(s) \approx \frac{-A}{s^2 + \gamma' s + \omega_r'^2}. \tag{24}$$

For a feedback loop requiring a phase margin of at least 30°, the relationship between the maximum allowable open-loop gain $K$ and the damping rate $\gamma'$ is governed by both the magnitude and phase conditions:

$$|H_o''(j\omega_c)| = 1, \quad \angle H_o''(j\omega_c) = -5\pi/6. \tag{25}$$

The gain $K$ is then obtained as

$$K = 4\zeta\left(\sqrt{3}\zeta + \sqrt{1 + 3\zeta^2}\right), \tag{26}$$

where $\omega_c$ is the gain crossover frequency at a phase of −150°, and $\zeta = \gamma'/(2\omega_r')$ is the damping ratio. Thus, in a second-order feedback system, a larger damping ratio permits a higher open-loop low-frequency gain $K$, leading to stronger noise suppression.

The noise suppression coefficient can be quantified as

$$\eta_{\mathrm{supp}} = \frac{1}{|1 + H_o''(s)|}. \tag{27}$$

And, at low frequencies, the noise suppression coefficient $\eta_{\mathrm{supp}} \approx 1/(1 + K)$. Under the damping enhancement by nonlinear crystal, phase and normalized gain curves are illustrated as curves (iii) and (vi) in Fig. 1, respectively. These two curves indicate that the corresponding gain at a 30° phase margin increases to 16 dB. Therefore, we find that nonlinear loss has the characteristic of increasing the maximum allowable open-loop gain of the feedback system by enhancing the damping of the laser, which makes it possible to suppress the low-frequency noise of all-solid-state lasers through optoelectronic feedback technology.

To more intuitively illustrate the influence of the open-loop gain and the nonlinear loss rate on the noise-suppression performance, we plot in Fig. 2 the calculated noise suppression coefficient $\eta_{\mathrm{supp}}$ as a function of frequency and these two key parameters, using the system parameters listed in Table 1. Here, $\eta_{\mathrm{supp}} = 0$ dB indicates no noise suppression, $\eta_{\mathrm{supp}} > 0$ dB indicates noise amplification, and $\eta_{\mathrm{supp}} < 0$ dB indicates effective suppression—the more negative $\eta_{\mathrm{supp}}$, the stronger the suppression capability.

Figure 2(a) shows the 3D plot of $\eta_{\mathrm{supp}}$ as a function of frequency and open-loop gain for a fixed nonlinear loss rate of $6 \times 10^6$ s$^{-1}$. It is evident that increasing the open-loop gain enhances the low-frequency noise suppression but simultaneously amplifies the resonant noise peak.

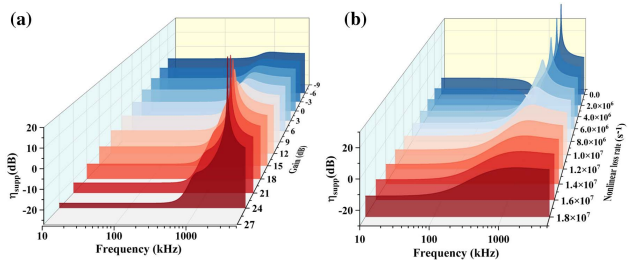



**Fig. 2.** Calculated noise suppression coefficient $\eta_{\mathrm{supp}}$ as a function of frequency and key feedback parameters. (a) 3D plot of $\eta_{\mathrm{supp}}$ versus frequency and open-loop gain $K$ for a fixed nonlinear loss rate of $2\kappa_n = 6 \times 10^6$ s$^{-1}$. (b) 3D plot of $\eta_{\mathrm{supp}}$ versus frequency and nonlinear loss rate $2\kappa_n$ for a fixed open-loop gain of $K = 15$ dB.

Figure 2(b) presents the 3D plot of $\eta_{\text{supp}}$ as a function of frequency and nonlinear loss rate for a fixed open-loop gain of 15 dB. Notably, increasing the nonlinear loss rate does not substantially change the low-frequency suppression level; instead, it enhances the damping of the resonant peak by increasing the phase margin, thereby allowing a higher allowable open-loop gain without sacrificing stability.

## 3. EXPERIMENTAL SETUP

Based on the above principles, we designed the experimental setup shown in Fig. 3, which comprises a low-noise all-solid-state single-frequency CW laser operating at 1064 nm and a pump-current optoelectronic feedback system incorporating both nonlinear loss and GaN-based high-bandwidth driving.

In the experimental system, the pump source is a fiber-coupled laser diode (LIMO-FP-A000748, Germany) with a center wavelength of 888 nm, a fiber core diameter of 400 μm, a numerical aperture of 0.22, and a maximum output power of 80.00 W. The pump beam is focused onto the gain crystal via a telescope coupling system comprising two plano–convex lenses ($f_1 = 30$ mm, $f_2 = 80$ mm) to achieve optimal mode matching between the pump beam and the laser resonator cavity mode [26]. The laser resonator adopts a four-mirror, figure-eight ring structure. Mirrors $M_1$ and $M_2$ are both concave–convex with a radius of curvature $R = 1500$ mm. $M_1$ is coated for high-transmittance (HT) film at 888 nm and high-reflectance (HR) film at 1064 nm, while $M_2$ is coated with HR film at 1064 nm. $M_3$ and the output coupler $M_4$ are both plano–concave mirrors with the radius of curvature $R = 100$ mm. $M_3$ is coated with HR film at 1064 nm, and $M_4$ is coated with HR film at 532 nm with a partial transmission of 20% at 1064 nm ($T_{1064\,\text{nm}} = 20\%$). The gain medium is an $a$-axis-cut composite $YVO_4$/Nd:$YVO_4$ crystal measuring 3 mm × 3 mm × (3 + 20) mm. The front 3-mm-long undoped $YVO_4$ substrate mitigates the thermal effects, while the rear 20-mm-long of Nd:$YVO_4$ substrate has a doping atomic percent of 0.8%. The rear facet of the gain crystal is wedged at 1.5° to introduce higher geometric loss for the $\sigma$-polarization, thereby ensuring that $\pi$-polarization dominates the cavity oscillation for stable, single-frequency operation. An optical isolator (OD), consisting of a terbium scandium

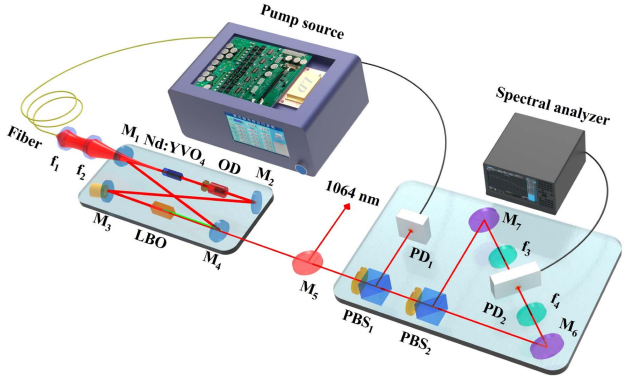



**Fig. 3.** Schematic of the experimental setup for the low-noise, single-frequency CW laser at 1064 nm.

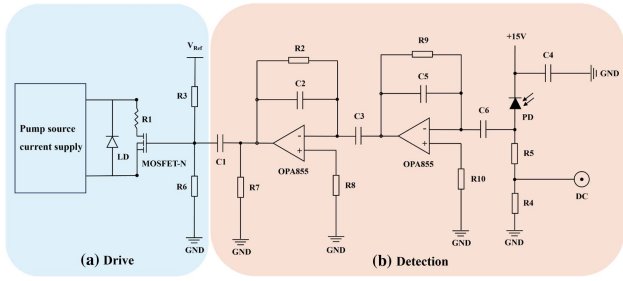



**Fig. 4.** Schematic diagram of the noise-suppression circuit implemented in the low-noise pump laser driver.

aluminum garnet (TSAG) crystal and a half-wave plate $\lambda/2$ is inserted to enforce unidirectional operation. For mode-hop-free single-frequency operation, a type I noncritically phase-matched LBO nonlinear crystal with 3 mm × 3 mm × 20 mm is placed at the fundamental mode beam waist between $M_3$ and $M_4$ to introduce nonlinear loss.

To effectively suppress noise at the low-frequency band of the laser, a portion of the laser beam is extracted from the main optical path using a polarizing beam splitter ($PBS_1$) and injected into a high-speed detector ($PD_1$). The detected signal of $PD_1$ is fed back to the high-speed driver of the LD to suppress the noise of the laser. Here, to achieve substantial noise suppression, the feedback signal must exhibit an ultra-low latency and an extremely high signal-to-noise ratio, which in turn requires both the $PD_1$ and the driver to possess high bandwidth and low noise. Accordingly, we designed the detection and driving circuitry illustrated in Fig. 4. The photodetector primarily consists of a high-speed photodiode, a transimpedance amplifier, and a voltage amplifier. The photodiode used is an FD100w, and the amplifiers are implemented with the OPA855, a device featuring a high gain-bandwidth product and a low parasitic capacitance. The current feedback driver circuit employs a high-speed GaN FET (EPC8004) connected in series with a power resistor R1. As a result, the photodetector achieves a response bandwidth of 10 Hz to 200 MHz, while the feedback driver operates with a bandwidth of 30 MHz.

The intensity noise of the laser is independently measured using a self-homodyne detection system. The beam transmitted through $PBS_1$ is divided into two equal parts by a polarizing beam splitter ($PBS_2$). The two beams of equal power are reflected by mirrors $M_6$ and $M_7$, focused by plano–convex lenses ($f_3$, $f_4$), and directed onto a photodetector ($PD_2$), which incorporates one InGaAs photodiode on each side. The effective measurement bandwidth of $PD_2$ is 100 Hz to 5 MHz. The output of $PD_2$ (YG2016-BHD01, Yuguang) is connected to a spectrum analyzer (N9040B, Keysight) to record the intensity noise spectrum.

## 4. EXPERIMENTAL RESULTS AND DISCUSSION

To evaluate the noise suppression performance of the proposed scheme and validate the theoretical model, we first characterized the key parameters of the experimental system. The RRO frequency of the free-running laser was measured to be approximately 710 kHz. In our setup, the 1064 nm fundamental

output power reaches as high as 30 W. At this power level, thermal effects and intracavity power-induced perturbations can aggravate the intrinsic mode competition of the homogeneously broadened gain. To prevent mode competition from destabilizing the output frequency and power, a weak nonlinear effect was introduced without affecting the RRO frequency, primarily by adjusting the temperature of the LBO crystal to reduce the second-harmonic conversion efficiency. Once stable output power was achieved, the intensity noise was measured using $PD_2$. The incident power on $PD_2$ was uniformly set to 2 mW. For the shot-noise reference measurement, 1 mW of optical power was directed onto each of the two photodiodes in the balanced detector; for laser intensity noise measurement, the full 2 mW was directed onto a single photodiode. The intensity noise spectrum of the free-running laser, normalized to SNL level, is shown as curve (i) in Fig. 5.

We first employed a conventional optoelectronic feedback system based on a silicon MOSFET driver with a response bandwidth of approximately 800 kHz. Experimentally, it was found that, even with very small feedback gain (<−10.4 dB), the RRO peak increased by more than 10 dB relative to the free-running laser, and the measured noise spectra fluctuated by up to ∼20 dB from trace to trace. In some cases, the feedback even induced mode hopping in the laser, making the system highly unstable and causing large fluctuations in the output noise. Consequently, the Si-based driver feedback introduced a large phase lag, which drove the loop toward positive feedback so that any applied gain amplified rather than suppressed the RRO.

Replacing the conventional driver with the designed GaN-based high-speed optoelectronic feedback circuit (shown in Fig. 4), we measured the noise spectral density under feedback control. When the open-loop gain of the feedback system was set to 0.3 (−10.4 dB) and 0.6 (−4.4 dB), the corresponding noise spectra measured by $PD_2$ were shown as curves (ii) and (iii) in Fig. 5, respectively. Compared with the ineffective suppression of the conventional feedback scheme, the high-speed GaN feedback circuit achieved approximately 4 dB of low-frequency noise suppression. However, the noise near the RRO frequency remained more than 10 dB higher than the low-frequency noise floor. Thus, while the high-speed optoelectronic feedback significantly improved the feedback stability of the laser, its low-frequency noise suppression capability remained limited.

To further validate the proposed optoelectronic synergistic noise suppression scheme, we increased the nonlinear conversion efficiency of the LBO crystal by finely controlling its temperature and slightly increased the LD current to achieve dual-wavelength operation with 30 W at 1064 nm and 1.65 W at 532 nm. Under this condition, the nonlinear loss rate could be calculated as $5.6 \times 10^6$/s based on the laser cavity design. Curve (i) in Fig. 6 presents the intensity noise spectrum of the 1064 nm laser without optoelectronic feedback, as measured by $PD_2$. Unlike the case without nonlinear loss, the laser with LBO-induced nonlinear loss exhibited almost no RRO peak, confirming that the LBO significantly increases the damping rate, as described by Eq. (23).

Then, we measured the closed loop feedback noise density spectrum with open-loop DC gains of −3.1, 3.5, 10.6, 14.3, and 16.8 dB, respectively, and the results are shown as curves (ii)–(vi) in Fig. 6. The corresponding low-frequency noise suppression levels were approximately $4.5 \pm 0.5$ dB, $7.2 \pm 0.5$ dB, $13.0 \pm 0.5$ dB, $16.0 \pm 0.5$ dB, and $18.4 \pm 0.5$ dB. These results clearly demonstrate that the introduction of nonlinear loss into the optoelectronic feedback system substantially enhances the noise suppression capability, thereby validating the effectiveness of the proposed optoelectronic synergistic noise suppression strategy.

Benefiting from the fact that nonlinear loss increases the damping rate and thus improves noise suppression, we further characterized the dependence of noise suppression on the damping ratio to provide technical guidance for the design of optoelectronic feedback systems. The damping ratio was adjusted by controlling the LBO temperature to vary the nonlinear conversion efficiency. Experimentally, we measured

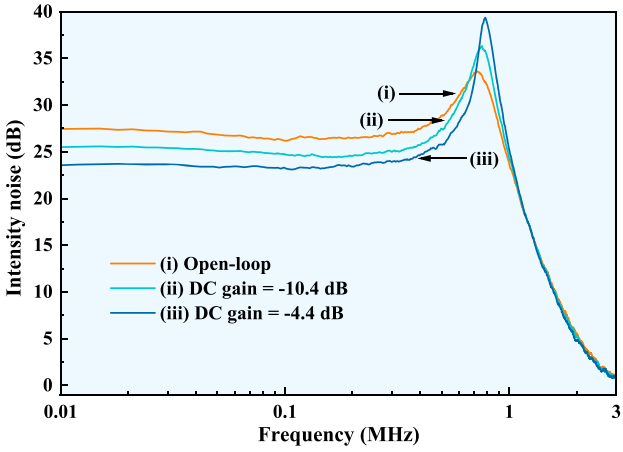



**Fig. 5.** Laser intensity noise spectra with GaN feedback circuit. Curve (i): free-running laser; curve (ii): with open-loop gain 0.3 (−10.4 dB); curve (iii): with open-loop gain 0.6 (−4.4 dB).

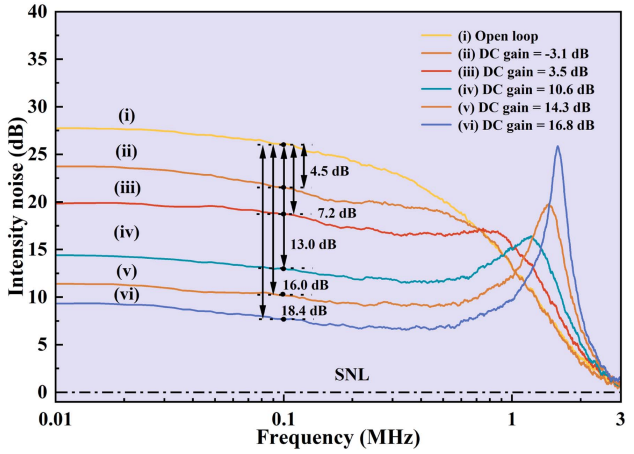



**Fig. 6.** Laser intensity noise spectra with nonlinear loss (30 W at 1064 nm, 1.65 W at 532 nm). Curve (i): free-running laser (no feedback); curves (ii)–(vi): with GaN-based feedback circuit at open-loop gains of −3.1, 3.5, 10.6, 14.3, and 16.8 dB, respectively. The corresponding low-frequency noise suppression levels are 4.5, 7.2, 13.0, 16.0, and 18.4 dB.

**Table 2. Comparison of Measured and Theoretical Noise Suppression at Different Nonlinear Loss Rates[a]**

| $2\kappa_n$ ($s^{-1}$) | $\zeta$ | $K_{meas}$ (dB) | $K_{theo}$ (dB) | $\eta_{supp,meas}$ (dB) | $\eta_{supp,theo}$ (dB) |
|---|---|---|---|---|---|
| $1.0 \times 10^6$ | 0.10 | −7.5 | −6.5 | $3.1 \pm 1.0$ | 3.4 |
| $2.5 \times 10^6$ | 0.25 | 3.0 | 3.7 | $7.5 \pm 1.0$ | 8.0 |
| $4.4 \times 10^6$ | 0.43 | 10.0 | 10.7 | $12.2 \pm 1.0$ | 12.9 |
| $5.6 \times 10^6$ | 0.55 | 14.3 | 14.2 | $16.0 \pm 1.0$ | 15.8 |

[a]The damping ratio $\zeta$ was determined from the measured RRO frequency and damping rate. The theoretical open-loop gain $K_{theo}$ is calculated from Eq. (26), and the theoretical noise suppression is $\eta_{supp,theo} = 20\log_{10}(1 + K_{theo})$. The measured gain $K_{meas}$ is the maximum value satisfying a 30° phase margin in the experiment.

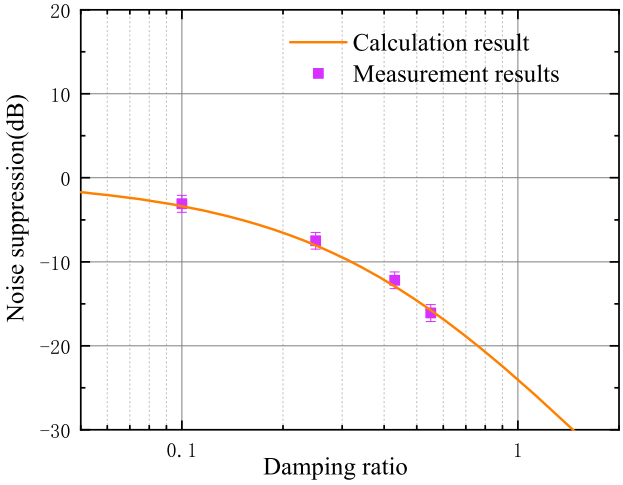



**Fig. 7.** Dependence of noise suppression on the damping ratio. Discrete points: experimental measurements; solid curve: theoretical prediction from Eq. (27).

noise suppression levels of $3.1 \pm 1.0$ dB, $7.5 \pm 1.0$ dB, $12.2 \pm 1.0$ dB, and $16.0 \pm 1.0$ dB at damping ratios of 0.1, 0.25, 0.43, and 0.55, respectively, with the corresponding nonlinear loss rates of $1.0 \times 10^6$, $2.5 \times 10^6$, $4.4 \times 10^6$, and $5.6 \times 10^6$ $s^{-1}$. The open-loop gain at each damping ratio was set to the maximum value satisfying a 30° phase margin. The theoretical gain $K_{theo}$ was calculated from Eq. (26), and the resulting theoretical suppression $\eta_{supp,theo} = 20\log_{10}(1 + K_{theo})$ agrees with the measured values within 1.5 dB (Table 2). These results are shown as discrete points in Fig. 7, together with the theoretical prediction of Eq. (27).

## 5. CONCLUSION

In this work, we have established a unified transfer function model for all-solid-state lasers with pump-current optoelectronic feedback. The developed model quantitatively links the laser's damping rate and feedback circuit bandwidth to the maximum allowable open-loop gain under a given phase margin [Eqs. (15) and (26)] and predicts the resulting low-frequency noise suppression [Eq. (27)]. Based on this relationship, we found that the fundamental bottleneck limiting the laser noise suppression capability is that the extremely small phase margin prevents any increase in the open-loop gain.

To overcome this limitation, we proposed and experimentally validated an optoelectronic synergistic approach that combined intracavity nonlinear loss with a high-bandwidth GaN-based feedback circuit. Theoretical analysis reveals a physical mechanism in which the nonlinear loss can increase the system damping rate to enhance the phase margin. When this combines with a broadband feedback circuit, the phase margin is further improved. The proposed model and approach were validated using an all-solid-state single-frequency CW 1064 nm laser with an output power of 30 W. With a GaN-based feedback circuit bandwidth of 30 MHz and a nonlinear loss rate of $5.6 \times 10^6$/s, low-frequency noise suppression exceeding 16 dB was achieved. This performance represents an order of magnitude improvement over that of conventional phase-advance compensation circuit optoelectronic-feedback methods. The experimental results showed excellent agreement with the theoretical predictions, indicating that further increasing the nonlinear loss is expected to bring the low-frequency noise close to the SNL.

Beyond this specific demonstration, this work provides a general design principle for integrated laser-and-feedback systems: engineering the damping of the laser can relax the gain-phase trade-off to enable higher feedback gain and noise suppression. This principle applies broadly to pump-current optoelectronic feedback systems, with direct implications for quantum optics, gravitational wave detection, cold atom physics, and precision metrology.

**Funding.** National Key Research and Development Program of China (2022YFC2204003); National Natural Science Foundation of China (62405170, 62575163).

**Disclosures.** The authors declare no conflicts of interest.

**Data Availability.** Data underlying the results presented in this paper are not publicly available at this time but may be obtained from the authors upon reasonable request.

## REFERENCES

1. B. P. Abbott, R. Abbott, T. D. Abbott, *et al.*, "Observation of gravitational waves from a binary black hole merger," Phys. Rev. Lett. **116**, 061102 (2016).
2. S. Tanioka, B. Wu, and S. W. Ballmer, "Experimental demonstration of frequency-downconverted arm-length stabilization for a future upgraded gravitational wave detector," Opt. Lett. **49**, 5763–5766 (2024).
3. F. Li, X. Shang, Z. Ma, *et al.*, "Laser intensity noise suppression for space-borne gravitational wave mission," Opt. Express **33**, 28141–28151 (2025).
4. F. Li, L. Tian, T. Huang, *et al.*, "Development of a low-intensity-noise laser source based on ultra-low-noise photodetectors in the sub-millihertz band," Opt. Laser Technol. **192**, 113747 (2025).
5. B. N. Markov, S. A. Babin, Z. Blaszczak, *et al.*, "High-resolution laser spectrometer for fundamental and applied research," Bull. Russ. Acad. Sci. Phys. **71**, 844–847 (2007).
6. K. K. Ni, S. Ospelkaus, D. Wang, *et al.*, "Dipolar collisions of polar molecules in the quantum regime," Nature **464**, 1324–1328 (2010).
7. X. Jia, Z. Yan, Z. Duan, *et al.*, "Experimental realization of three-color entanglement at optical fiber communication and atomic storage wavelengths," Phys. Rev. Lett. **109**, 253604 (2012).
8. M. Huo, J. Qin, J. Cheng, *et al.*, "Deterministic quantum teleportation through fiber channels," Sci. Adv. **4**, eaas9401 (2018).

9. T. Heindel, J.-H. Kim, N. Gregersen, *et al.*, "Quantum dots for photonic quantum information technology," Adv. Opt. Photonics **15**, 613–738 (2023).
10. J. Miao, G. Bian, B. Shan, *et al.*, "Achieving ultracold Bose-Fermi mixture of $^{87}$Rb and $^{40}$K with dual dark magnetic-optical-trap," Chin. Phys. B **31**, 080306 (2022).
11. B. Shan, L. Huang, Y. Zhao, *et al.*, "Chiral Raman coupling for spin-orbit coupling in ultracold atomic gases," Phys. Rev. A **111**, 023323 (2025).
12. Y. Yamamoto, S. Machida, and O. Nilsson, "Amplitude squeezing in a pump-noise-suppressed laser oscillator," Phys. Rev. A **34**, 4025–4042 (1986).
13. T. Kane, "Intensity noise in diode-pumped single-frequency Nd:YAG lasers and its control by electronic feedback," IEEE Photonics Technol. Lett. **2**, 244–245 (1990).
14. A. M. van der Lee, N. J. van Druten, M. P. van Exter, *et al.*, "Critical Petermann *K* factor for intensity noise squeezing," Phys. Rev. Lett. **85**, 4711–4714 (2000).
15. Y. Xiao, C. Li, S.-H. Xu, *et al.*, "Simultaneously suppressing low-frequency and relaxation oscillation intensity noise in a DBR single-frequency phosphate fiber laser," Chin. Phys. Lett. **32**, 064205 (2015).
16. J. Zhang, S. Wei, H. Liu, *et al.*, "Measurement technique for broadband frequency and intensity noise of single-frequency laser," Chin. J. Lasers **48**, 0301002 (2021).
17. Y. Wang, K. Wang, E. F. Fenton, *et al.*, "Reduction of laser intensity noise over 1 MHz band for single atom trapping," Opt. Express **28**, 31209–31215 (2020).
18. R. Li, N. Jiao, B. An, *et al.*, "Quantum-enhanced laser phase noise filter," Optica **13**, 297–302 (2026).
19. C. Cahillane, G. L. Mansell, and D. Sigg, "Laser frequency noise in next generation gravitational-wave detectors," Opt. Express **29**, 42144–42161 (2021).
20. A. E. Amili and M. Alouini, "Noise reduction in solid-state lasers using a SHG-based buffer reservoir," Opt. Lett. **40**, 1149–1152 (2015).
21. Y. Guo, H. Lu, W. Peng, *et al.*, "Intensity noise suppression of a high-power single-frequency CW laser by controlling the stimulated emission rate," Opt. Lett. **44**, 6033–6036 (2019).
22. C. C. Harb, T. C. Ralph, E. H. Huntington, *et al.*, "Intensity-noise dependence of Nd:YAG lasers on their diode-laser pump source," J. Opt. Soc. Am. B **14**, 2936–2945 (1997).
23. J. Zhang, Y. Cheng, T. Zhang, *et al.*, "Investigation of the characteristics of the intensity noise of singly resonant active second-harmonic generation," J. Opt. Soc. Am. B **17**, 1695–1703 (2000).
24. J. Zhang, H. Ma, R. Wang, *et al.*, "Suppression of intensity noise of LD-pumped single-frequency ring Nd:$YVO_4$ lasers by opto-electronic feedback," Acta Opt. Sin. **21**, 1031–1035 (2001).
25. J. Zhang, H. Chang, X. Jia, *et al.*, "Suppression of the intensity noise of a laser-diode-pumped single-frequency ring Nd:$YVO_4$–KTP green laser by optoelectronic feedback," Opt. Lett. **26**, 695–697 (2001).
26. Y.-F. Chen, "Pump-to-mode size ratio dependence of thermal loading in diode-end-pumped solid-state lasers," J. Opt. Soc. Am. B **17**, 1835–1840 (2000).